# Breaking linear scaling relationships with transition metal carbides

Hector Prats and Michail Stamatakis

*Department of Chemical Engineering, University College London, Roberts Building, Torrington Place, London WC1E 7JE, UK*

Corresponding author: Hector Prats (h.garcia@ucl.ac.uk)

## S1. Computational Details

Periodic spin polarised DFT calculations were performed using the Vienna *Ab-initio* Simulation Package (VASP), version 5.4.4.[1] The PBE exchange correlation functional[2] was used, which has been demonstrated to provide most accurate results among GGA functionals in describing the atomic and electronic structure of TMCs.[3] Dispersion (van der Waals) interactions were included through the D3 method as proposed by Grimme and coworkers.[4] Plane-wave kinetic energy cutoffs of 520 eV and 415 eV were used for bulk and surface calculations, respectively, and the core electrons were accounted for using the projector-augmented wave (PAW) method.[5,6] The bulk structures for all TMs and TMCs were obtained from the Materials Project open dataset[7] (see Table S1).

For bulk geometry relaxation, electronic and force convergence tolerances of $10^{-6}$ eV and $10^{-3}$ eV·Å$^{-1}$, respectively, were imposed, and a dense $\Gamma-$ centred k-point grid of $80/a \times 80/b \times 80/c$ was used, with non-integer values rounded up to the nearest integer. The slab models for the surfaces were constructed from the optimised bulk structures. For the relaxation of the clean slabs, adsorbed configurations, and transition state calculations, electronic and force convergence tolerances of $10^{-5}$ eV and $10^{-2}$ eV·Å$^{-1}$, respectively, were imposed, and a $\Gamma-$ centred k-point grid of $60/a \times 60/b \times 1$ was used, with non-integer values rounded up to the nearest integer. For the calculation of the density of states (DOS) for the slab models, a denser $\Gamma-$ centred k-point grid of $120/a \times 120/b \times 1$ was used. For all systems, the bottom half of the slab in the vertical z-direction was constrained at the bulk positions, while the top half of the slab, the metal clusters and the adsorbed species were fully relaxed. A supercell of 27 Å in the z-direction was used for all slab calculations, ensuring that periodic slab images were separated by at least 18 Å of vacuum, and a dipole correction was applied. All crystal structure manipulations and data analysis were carried out using the Python Materials Genomics package (pymatgen)[8] and the Atomic Simulation Environment (ASE).[9]

Optimised structures (VASP CONTCAR files) for all geometry optimisations performed in this work have been made available on a public GitHub repository: https://github.com/hprats/Adsorption-transition-metal-carbides

**Table S1.** Experimental and calculated lattice parameters for the bulk TMCs and TMs. For Co and Ni, the calculated magnetic moments per atom are 1.61 and 0.61 $\mu_B$, respectively, which agree well with the experimental values of 1.7 and 0.6 $\mu_B$.[10]

| Structure | Materials Project ID | Lattice parameters (a, b, c) / Å* | | Deviation / % |
|---|---|---|---|---|
| | | Experimental | Calculated (PBE-D3) | |
| TiC | mp-631 | 4.328[11] | 4.308 | -0.46 |
| ZrC | mp-2795 | 4.698[12] | 4.694 | -0.08 |
| HfC | mp-21075 | 4.631[11] | 4.624 | -0.16 |
| VC | mp-1282 | 4.165[11] | 4.138 | -0.65 |
| NbC | mp-910 | 4.469[13] | 4.460 | -0.21 |
| TaC | mp-1086 | 4.453[11] | 4.456 | 0.07 |
| h − MoC | mp-2305 | 2.898, 2.898, 2.809[14] | 2.904, 2.904, 2.819 | 0.22, 0.22, 0.34 |
| c − MoC | mp-2746 | 4.278[15] | 4.348 | 1.63 |
| h − WC | mp-1894 | 2.91, 2.91, 2.84[16] | 2.913, 2.913, 2.846 | 0.11, 0.11, 0.20 |
| c − WC | mp-13136 | 4.374[17] | 4.366 | -0.19 |
| Rh | mp-74 | 3.803[18] | 3.812 | 0.23 |
| Pd | mp-2 | 3.890[19] | 3.899 | 0.23 |
| Pt | mp-126 | 3.924[20] | 3.927 | 0.08 |
| Au | mp-81 | 4.079[21] | 4.116 | 0.91 |
| Co | mp-54 | 2.507, 2.507, 4.069[22] | 2.472, 2.472, 2.472 | -1.38, -1.38, -1.85 |
| Ni | mp-23 | 3.524[23] | 3.483 | -1.17 |
| Cu | mp-30 | 3.615[24] | 3.569 | -1.26 |

* If a = b = c only one value is indicated

**S2. Formation energy**

The formation energy ($E_f$) of each adsorbed species is defined relative to the clean slab and a common set of gas-phase molecules ($H_{2(g)}$, $CH_{4(g)}$ and $CO_{2(g)}$), thereby allowing the stability of different fragments to be compared to one another within the same reference. In the case of a generic adsorbate $i$, $E_f$ is computed as:

$$E_f = E_{i+slab} - E_{slab} - \sum_j n_j R_j \quad (4)$$

where $E_{i+slab}$ is the total energy of the slab with adsorbate $i$, $E_{slab}$ is the total energy of the clean slab, $n_j$ is the number of atomic species $j$ ($j =$ H, C or O) in adsorbate $i$, and $R_j$ is the reference energy of that atomic species, defined in our reference set as:

$$R_H = \frac{1}{2}E_{H_{2(g)}} \quad (5)$$

$$R_C = E_{CH_{4(g)}} - 4R_H \quad (6)$$

$$R_O = \frac{1}{2}\left(E_{CO_{2(g)}} - R_C\right) \quad (7)$$

With this definition, more negative values of $E_f$ imply higher stability of the adsorbed configurations they correspond to. Also, the formation energies for the reference $H_{2(g)}$, $CH_{4(g)}$ and $CO_{2(g)}$ molecules correspond to their adsorption energies. Table S2 contains all reference values used in this work, which enable the conversion of all $E_f$ values reported in this work to total DFT energies.

**Table S2.** Tabulated energies for the reference set used to obtain all $E_f$ used in this work.

| Species | $R_i$ (eV) | TM slab | $E_{slab}$ (eV) | TMC slab | $E_{slab}$ (eV) |
|---|---|---|---|---|---|
| H | -3.38 | Rh(111) | -470.56 | TiC(001) | -1198.29 |
| C | -10.51 | Pd(111) | -340.43 | ZrC(001) | -1230.74 |
| O | -6.24 | Pt(111) | -403.79 | HfC(001) | -1335.11 |
| | | Au(111) | -230.20 | VC(001) | -1230.60 |
| | | Co(0001) | -447.69 | NbC(001) | -1310.79 |
| | | Ni(111) | -354.49 | TaC(001) | -1418.45 |
| | | Cu(111) | -246.23 | cMoC(001) | -1275.30 |
| | | | | cWC(001) | -1390.12 |
| | | | | hMoC(001)-Mo | -1139.69 |
| | | | | hWC(001)-W | -1267.74 |
| | | | | hMoC(001)-C | -1052.73 |

**S3. Dataset**

For all TMCs under consideration except MoC and WC, we have only considered the most stable phase, which corresponds to a *fcc* crystal packing, with the (001) facet being the lowest energy one.[25] For MoC[26] and WC,[27,28] *fcc* and *hcp* phases can be synthesised with high stability, so both phases are considered. The (001) facet is the lowest energy one for *fcc* MoC[29] and WC,[25] while the most stable facet for their *hcp* phase is the (0001).[27,29] Note that the latter can be terminated with metal atoms or C atoms. For hcp MoC, both Mo- and C-terminated (0001) facets have been theoretically predicted to have similar stability[29] and are included in this study, while for hcp WC, the W-terminated (0001) face is significantly more stable than the C-terminated (0001) one,[27] so only the C-termination is considered. To ease the notation, the cubic *fcc* and hexagonal *hcp* phases for MoC and WC are referred to as cTMC and hTMC, respectively. The size of the metal cluster is 4 atoms on cTMCs and 3 atoms on hTMCs. These sizes feature compact, high symmetry structures that maximise the atomic coordination with the support and are thus likely to be energetically stable. Moreover, previous experimental[30,31,32] and theoretical[33,34,35] studies have shown that the activity is higher when the size of these nanoclusters is very small (<0.6 nm). Finally, for each $TM_n$@TMC system, the supported cluster can adopt many different configurations (Figure S1). In our previous work,[36] we determined the most stable configuration for each one of the $TM_n$@TMCs. Here, we consider the most stable configuration for each cluster except if it corresponds to a 3D configuration (i.e., tetrahedral), which is the case for 8 systems. In these cases, the high variety of adsorption sites triggers the complexity of the screening, so we consider their most stable 2D configuration, which in most cases has a similar stability to the tetrahedral one (Table S3). Finally, we note that, while the most stable facet for TMs or TMCs is not necessarily the most reactive one,[37] large catalyst nanoparticles will predominantly exhibit the most stable facet, so it is usually taken as a typical benchmark for catalytic studies.

**Table S3.** List of $TM_n$@TMCs for which the most stable configuration is 3D (i.e., tetrahedral), and relative stability to the most stable 2D configuration (i.e., square).

| Cluster | Most stable 2D configuration (Figure S1) | Stability of the 2D configuration compared to the 3D one (eV) |
|---|---|---|
| $Au_n$@TiC | tC-M | 0.29 |
| $Au_n$@ZrC | tC-M | 0.06 |
| $Au_n$@HfC | tC-M | 0.18 |
| $Au_n$@cMoC | br-C | 0.23 |
| $Pt_n$@cMoC | tC-M | 0.23 |
| $Au_n$@cWC | br-C | 0.31 |
| $Cu_n$@cWC | br-C | 0.14 |
| $Pt_n$@cWC | tC-M | 0.64 |

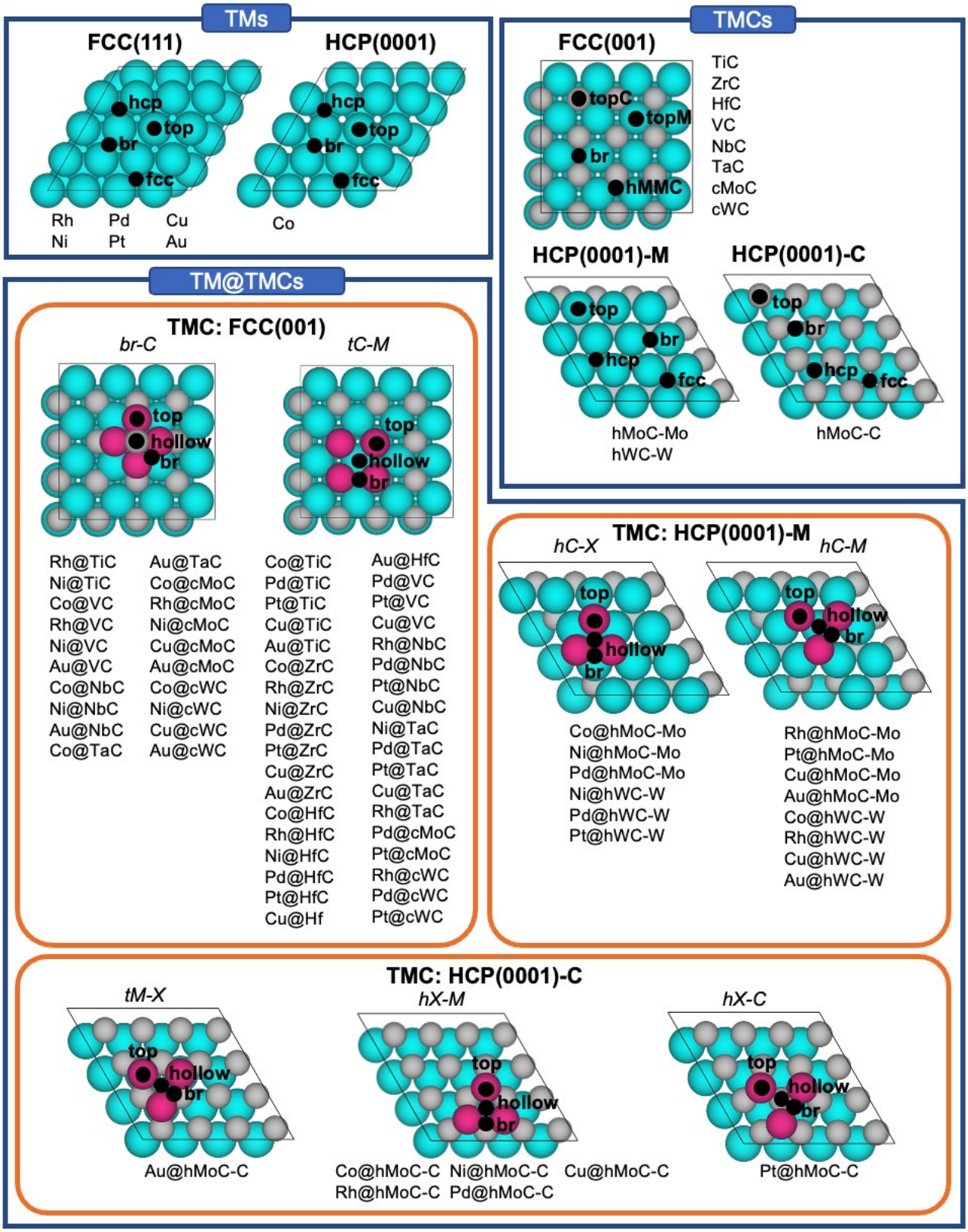


**Figure S1.** Classification of all systems screened in this study and the corresponding adsorption sites for each type of system. For TM@TMCs, the cluster configuration is shown in italics, following the notation from Ref. 36.

**S4. Results**

**Table S4.** Calculated formation energies for the different adsorbed species on TM slabs. Only the most stable adsorption site is considered.

| TM | Formation energy (eV) | | | | | | | | | | |
|---|---|---|---|---|---|---|---|---|---|---|---|
| | C | CH | $CH_2$ | $CH_3$ | $CH_4$ | CO | $CO_2$ | H | $H_2O$ | O | OH |
| Rh(111) | 1.73 | 0.84 | 0.80 | 0.35 | -0.22 | -0.23 | -0.26 | -0.58 | -1.76 | -0.78 | -1.11 |
| Pd(111) | 2.23 | 1.23 | 1.16 | 0.47 | -0.25 | -0.24 | -0.29 | -0.64 | -1.68 | -0.04 | -0.66 |
| Pt(111) | 1.88 | 0.76 | 0.80 | 0.12 | -0.27 | -0.13 | -0.31 | -0.55 | -1.70 | 0.07 | -0.49 |
| Au(111) | 4.58 | 3.06 | 2.35 | 0.96 | -0.22 | 1.47 | -0.25 | 0.10 | -1.54 | 1.17 | -0.12 |
| Co(0001) | 2.17 | 1.21 | 0.89 | 0.11 | -0.23 | 0.10 | -0.20 | -0.64 | -1.74 | -1.35 | -1.72 |
| Ni(111) | 2.26 | 1.15 | 0.85 | 0.15 | -0.26 | -0.14 | -0.22 | -0.66 | -1.76 | -1.07 | -1.51 |
| Cu(111) | 4.11 | 2.55 | 1.78 | 0.63 | -0.27 | 0.82 | -0.23 | -0.37 | -1.66 | -0.34 | -1.23 |

**Table S5.** Calculated formation energies for the different adsorbed species on TMC slabs. Only the most stable adsorption site is considered.

| TMC | Formation energy (eV) | | | | | | | | | | |
|---|---|---|---|---|---|---|---|---|---|---|---|
| | C | CH | $CH_2$ | $CH_3$ | $CH_4$ | CO | $CO_2$ | H | $H_2O$ | O | OH |
| TiC(001) | 2.05 | 1.08 | 0.98 | 0.16 | -0.24 | 0.30 | -0.77 | -0.54 | -1.88 | -1.15 | -0.82 |
| ZrC(001) | 2.20 | 1.47 | 0.72 | 0.22 | -0.25 | 0.01 | -1.54 | -0.64 | -1.94 | -1.39 | -1.27 |
| HfC(001) | 2.48 | 1.68 | 0.90 | 0.30 | -0.25 | 0.29 | -1.59 | -0.56 | -2.00 | -1.30 | -1.48 |
| VC(001) | 2.10 | 1.15 | 1.39 | 0.71 | -0.23 | 0.83 | -0.26 | 0.04 | -1.81 | -0.82 | -0.86 |
| NbC(001) | 2.75 | 1.87 | 1.37 | 0.81 | -0.20 | 0.62 | -0.88 | 0.09 | -1.88 | -1.44 | -1.69 |
| TaC(001) | 2.81 | 1.71 | 1.46 | 0.40 | -0.25 | 0.69 | -1.17 | -0.06 | -1.99 | -1.82 | -2.09 |
| cMoC(001) | 1.47 | 0.38 | 0.45 | -0.29 | -0.95 | -0.22 | -1.33 | -0.59 | -2.59 | -1.68 | -1.00 |
| cWC(001) | 1.89 | 0.42 | 0.40 | -0.65 | -1.18 | -0.06 | -1.66 | -1.00 | -2.91 | -1.82 | -1.58 |
| hMoC(001)-Mo | 1.63 | 0.36 | -0.01 | -0.54 | -0.19 | 0.08 | -1.33 | -0.95 | -1.98 | -3.32 | -2.82 |
| hWC(001)-W | 1.67 | 0.13 | -0.27 | -0.77 | -0.23 | -0.05 | -1.16 | -1.05 | -2.05 | -3.34 | -2.79 |
| hMoC(001)-C | -0.22 | -0.13 | -0.33 | -1.03 | -0.19 | -0.60 | -1.51 | -1.32 | -1.74 | -2.04 | -1.15 |

**Table S6.** Calculated formation energies for the different adsorbed species on TM@TMC. Only the most stable adsorption site is considered.

| TM@TMC | Formation energy (eV) | | | | | | | | | | |
|---|---|---|---|---|---|---|---|---|---|---|---|
| | C | CH | $CH_2$ | $CH_3$ | $CH_4$ | CO | $CO_2$ | H | $H_2O$ | O | OH |
| Au@cMoC | 3.65 | 2.35 | 1.20 | 0.24 | -0.26 | 0.53 | -0.32 | -0.36 | -1.81 | 0.31 | -1.19 |
| Co@cMoC | 2.23 | 0.82 | 0.26 | -0.34 | -0.18 | -0.07 | -0.18 | -1.03 | -1.73 | -1.37 | -1.43 |
| Cu@cMoC | 1.49 | 0.98 | 0.60 | -0.43 | -0.56 | 0.07 | -0.60 | -1.00 | -2.30 | -1.37 | -2.14 |
| Ni@cMoC | 2.16 | 1.06 | 0.55 | -0.21 | -0.19 | 0.12 | -0.17 | -0.89 | -1.70 | -1.38 | -1.35 |
| Pd@cMoC | 3.23 | 2.31 | 1.26 | 0.13 | -0.64 | 0.03 | -0.59 | -0.67 | -2.11 | -0.33 | -1.79 |
| Pt@cMoC | 2.38 | 1.47 | 0.51 | -0.23 | -0.83 | -0.69 | -0.60 | -0.86 | -2.31 | -0.72 | -1.98 |
| Rh@cMoC | 2.14 | 0.42 | 0.15 | -0.43 | -0.22 | -0.24 | -0.25 | -0.90 | -1.80 | -1.89 | -1.60 |
| Au@cWC | 3.81 | 2.11 | 0.95 | -0.24 | -0.44 | 0.13 | -0.50 | -0.62 | -2.22 | -0.12 | -1.39 |
| Co@cWC | 1.83 | 0.41 | -0.02 | -0.61 | -0.44 | -0.28 | -0.40 | -1.25 | -2.17 | -1.43 | -1.57 |
| Cu@cWC | 2.04 | 0.66 | 0.56 | -0.46 | -0.75 | -0.10 | -0.75 | -1.22 | -2.43 | -1.50 | -2.35 |
| Ni@cWC | 1.23 | 0.37 | 0.20 | -0.75 | -1.06 | -0.68 | -0.92 | -1.35 | -2.67 | -1.96 | -2.35 |
| Pd@cWC | 3.26 | 2.02 | 1.00 | -0.08 | -0.94 | -0.30 | -1.05 | -1.00 | -2.50 | -0.79 | -1.95 |
| Pt@cWC | 2.11 | 1.07 | -0.10 | -0.81 | -1.24 | -0.99 | -1.12 | -1.81 | -2.68 | -1.26 | -2.45 |
| Rh@cWC | 1.37 | 1.22 | 0.55 | -0.29 | -0.75 | -0.44 | -1.40 | -0.61 | -2.29 | -0.78 | -2.03 |
| Au@hMoC-C | 4.02 | 2.12 | 1.19 | 0.20 | -0.29 | 0.52 | -0.19 | -0.35 | -2.06 | -0.53 | -1.59 |
| Co@hMoC-C | 3.42 | 2.68 | 1.66 | 0.44 | -0.48 | 0.09 | -0.35 | -0.44 | -2.23 | -0.58 | -1.59 |
| Cu@hMoC-C | 2.25 | 3.06 | 1.89 | 0.52 | -0.40 | 0.56 | -0.40 | -0.11 | -2.14 | -0.40 | -1.99 |
| Ni@hMoC-C | 3.03 | 1.59 | 1.98 | 0.65 | -0.42 | 0.29 | -0.29 | 0.01 | -2.13 | -0.18 | -1.41 |
| Pd@hMoC-C | 4.85 | 3.63 | 2.29 | 0.80 | -0.33 | 0.50 | -0.23 | -0.19 | -2.04 | 0.42 | -1.12 |
| Pt@hMoC-C | 0.12 | -0.07 | -1.81 | -2.64 | -1.98 | 0.04 | -1.90 | -0.46 | -3.55 | -3.84 | -2.32 |
| Rh@hMoC-C | 4.19 | 2.76 | 1.71 | 0.53 | -0.35 | 0.33 | -0.25 | -0.68 | -2.12 | -0.09 | -1.33 |
| Au@hMoC-Mo | 4.05 | 2.85 | 1.68 | 0.46 | -0.14 | 0.47 | -0.18 | -0.07 | -1.63 | -0.92 | -1.34 |
| Co@hMoC-Mo | 1.91 | 0.86 | 0.17 | -0.52 | -0.35 | -0.31 | -1.21 | -0.84 | -2.08 | -2.50 | -2.85 |
| Cu@hMoC-Mo | 1.72 | 2.15 | 1.15 | 0.36 | -0.30 | 0.61 | -0.22 | -0.37 | -2.02 | -1.35 | -1.90 |
| Ni@hMoC-Mo | 1.82 | 1.31 | 0.53 | -0.04 | -0.32 | 0.11 | -0.35 | -0.67 | -1.96 | -1.88 | -2.36 |
| Pd@hMoC-Mo | 2.74 | 2.85 | 1.83 | 0.62 | -0.20 | 0.66 | -0.21 | -0.34 | -1.78 | -0.11 | -1.47 |
| Pt@hMoC-Mo | 1.67 | 1.84 | 1.23 | 0.23 | -0.22 | 0.23 | -0.23 | -0.38 | -1.76 | -0.63 | -1.48 |
| Rh@hMoC-Mo | 1.43 | 0.63 | 1.36 | 0.47 | -0.26 | -0.36 | -0.22 | -0.40 | -1.84 | -0.83 | -1.73 |
| Au@hWC-W | 3.99 | 2.86 | 1.57 | 0.36 | -0.27 | 0.81 | -0.21 | -0.17 | -1.78 | -0.82 | -1.31 |
| Co@hWC-W | 0.62 | 0.42 | 0.24 | -0.45 | -0.52 | -0.34 | -1.44 | -0.90 | -2.10 | -2.54 | -2.80 |
| Cu@hWC-W | 1.88 | 2.27 | 1.09 | 0.18 | -0.39 | 0.55 | -0.26 | -0.50 | -2.10 | -1.36 | -2.04 |
| Ni@hWC-W | 2.70 | 1.31 | 0.50 | -0.09 | -0.41 | 0.03 | -0.85 | -0.73 | -2.05 | -1.87 | -2.41 |
| Pd@hWC-W | 2.84 | 2.85 | 1.84 | 0.61 | -0.25 | 0.66 | -0.24 | -0.33 | -1.86 | -0.04 | -1.47 |
| Pt@hWC-W | 2.98 | 2.01 | 1.25 | 0.23 | -0.27 | 0.32 | -0.26 | -0.47 | -1.83 | -0.44 | -1.54 |
| Rh@hWC-W | 1.28 | 0.45 | 1.27 | 0.34 | -0.30 | 0.24 | -0.26 | -0.58 | -1.91 | -0.96 | -1.83 |
| Au@HfC | 4.00 | 2.03 | 0.95 | -0.08 | -0.16 | 0.39 | -0.22 | -0.68 | -1.84 | -0.11 | -1.59 |
| Co@HfC | 0.95 | 0.61 | 0.37 | -0.18 | -0.28 | -0.21 | -1.10 | -0.79 | -1.87 | -2.17 | -2.32 |
| Cu@HfC | 2.60 | 0.78 | 0.53 | 0.10 | -0.28 | 0.49 | -0.24 | -0.56 | -1.92 | -1.65 | -2.08 |
| Ni@HfC | 0.41 | 0.16 | 0.00 | -0.54 | -0.46 | -0.80 | -1.65 | -1.09 | -2.05 | -2.28 | -2.62 |

| | | | | | | | | | | | |
|---|---|---|---|---|---|---|---|---|---|---|---|
| Pd@HfC | 2.40 | 1.86 | 1.33 | 0.07 | -0.45 | -0.01 | -0.84 | -0.71 | -1.89 | -0.62 | -1.95 |
| Pt@HfC | 2.00 | 1.37 | 0.70 | -0.26 | -0.43 | -0.51 | -0.77 | -0.89 | -2.04 | -0.87 | -2.13 |
| Rh@HfC | 0.84 | 0.70 | 0.57 | 0.19 | -0.44 | -0.33 | -0.92 | -0.50 | -1.89 | -1.29 | -1.89 |
| Au@NbC | 4.29 | 2.77 | 1.34 | 0.39 | -0.14 | 0.81 | -0.20 | -0.17 | -1.58 | 0.53 | -0.95 |
| Co@NbC | 2.43 | 1.07 | 0.82 | 0.39 | -0.15 | 0.33 | -0.18 | -0.44 | -1.61 | -0.97 | -1.38 |
| Cu@NbC | 2.46 | 0.90 | 0.94 | 0.02 | -0.26 | 0.41 | -0.22 | -0.62 | -1.89 | -1.24 | -2.09 |
| Ni@NbC | 2.02 | 1.18 | 0.72 | 0.12 | -0.18 | 0.32 | -0.18 | -0.70 | -1.61 | -0.79 | -1.15 |
| Pd@NbC | 2.96 | 1.92 | 1.49 | 0.31 | -0.32 | 0.15 | -0.29 | -0.48 | -1.85 | -0.29 | -1.63 |
| Pt@NbC | 2.67 | 1.57 | 0.73 | 0.04 | -0.34 | -0.44 | -0.31 | -0.57 | -1.98 | -0.63 | -1.74 |
| Rh@NbC | 1.24 | 0.95 | 0.99 | 0.00 | -0.40 | -0.34 | -1.12 | -0.67 | -1.91 | -0.96 | -1.96 |
| Au@TaC | 4.49 | 2.97 | 1.14 | 0.11 | -0.14 | 0.72 | -0.21 | -0.52 | -1.53 | 0.56 | -0.87 |
| Co@TaC | 2.18 | 0.85 | 0.62 | 0.18 | -0.30 | 0.13 | -0.30 | -0.66 | -1.76 | -1.14 | -1.58 |
| Cu@TaC | 2.43 | 0.91 | 1.00 | 0.00 | -0.29 | 0.34 | -0.23 | -0.73 | -1.91 | -1.10 | -2.07 |
| Ni@TaC | 1.08 | 0.30 | 0.14 | -0.23 | -0.44 | -0.23 | -1.22 | -0.82 | -2.03 | -1.79 | -2.30 |
| Pd@TaC | 2.91 | 1.77 | 1.37 | 0.26 | -0.33 | 0.10 | -0.30 | -0.51 | -1.87 | -0.38 | -1.66 |
| Pt@TaC | 2.57 | 1.36 | 0.58 | -0.09 | -0.36 | -0.54 | -0.32 | -0.64 | -2.02 | -0.73 | -1.82 |
| Rh@TaC | 1.27 | 0.84 | 0.77 | -0.10 | -0.45 | -0.34 | -1.15 | -0.76 | -1.96 | -1.15 | -2.10 |
| Au@TiC | 3.96 | 2.13 | 1.07 | -0.10 | -0.22 | 0.35 | -0.22 | -0.68 | -1.89 | 0.03 | -1.47 |
| Co@TiC | 1.09 | 0.88 | 0.55 | -0.21 | -0.38 | -0.17 | -0.96 | -0.95 | -1.88 | -1.90 | -2.32 |
| Cu@TiC | 2.73 | 0.91 | 0.53 | 0.09 | -0.36 | 0.45 | -0.26 | -0.48 | -1.98 | -1.62 | -2.03 |
| Ni@TiC | 1.76 | 0.95 | 0.76 | -0.02 | -0.33 | 0.18 | -0.22 | -0.86 | -1.92 | -1.35 | -2.07 |
| Pd@TiC | 2.40 | 2.10 | 1.50 | 0.20 | -0.48 | -0.02 | -0.83 | -0.67 | -1.94 | -0.24 | -1.77 |
| Pt@TiC | 2.11 | 1.60 | 0.87 | -0.16 | -0.45 | -0.54 | -0.67 | -0.79 | -2.00 | -0.62 | -1.94 |
| Rh@TiC | 3.12 | 1.90 | 1.18 | 0.25 | -0.22 | 0.16 | -0.22 | -0.41 | -1.78 | -0.84 | -1.82 |
| Au@VC | 3.99 | 2.32 | 1.26 | 0.36 | -0.13 | 0.81 | -0.20 | -0.29 | -1.64 | 0.46 | -1.12 |
| Co@VC | 1.84 | 0.82 | 0.52 | 0.05 | -0.22 | 0.12 | -0.18 | -0.73 | -1.79 | -1.20 | -1.56 |
| Cu@VC | 2.63 | 1.09 | 0.88 | 0.01 | -0.33 | 0.44 | -0.23 | -0.59 | -1.92 | -1.25 | -2.06 |
| Ni@VC | 1.99 | 0.94 | 0.54 | -0.02 | -0.20 | 0.11 | -0.17 | -0.80 | -1.73 | -0.99 | -1.08 |
| Pd@VC | 3.00 | 2.24 | 1.56 | 0.37 | -0.41 | 0.10 | -0.49 | -0.60 | -1.88 | -0.16 | -1.50 |
| Pt@VC | 2.75 | 1.89 | 0.87 | 0.00 | -0.48 | -0.56 | -0.38 | -0.52 | -2.03 | -0.40 | -1.56 |
| Rh@VC | 2.03 | 0.63 | 0.45 | 0.16 | -0.23 | -0.14 | -0.20 | -0.57 | -1.75 | -1.64 | -1.30 |
| Au@ZrC | 4.06 | 2.13 | 1.04 | 0.05 | -0.15 | 0.43 | -0.22 | -0.55 | -1.82 | -0.06 | -1.51 |
| Co@ZrC | 0.90 | 0.60 | 0.36 | -0.17 | -0.27 | -0.22 | -1.11 | -0.80 | -1.86 | -2.20 | -2.32 |
| Cu@ZrC | 2.64 | 0.85 | 0.55 | 0.15 | -0.27 | 0.50 | -0.23 | -0.48 | -1.91 | -1.65 | -2.05 |
| Ni@ZrC | 0.37 | 0.10 | 0.01 | -0.49 | -0.45 | -0.83 | -1.64 | -1.09 | -2.03 | -2.33 | -2.60 |
| Pd@ZrC | 2.27 | 1.75 | 1.33 | 0.12 | -0.44 | 0.00 | -0.83 | -0.68 | -1.87 | -0.64 | -1.91 |
| Pt@ZrC | 1.90 | 1.30 | 0.76 | -0.21 | -0.41 | -0.48 | -0.77 | -0.86 | -2.00 | -0.86 | -2.09 |
| Rh@ZrC | 0.80 | 0.60 | 0.55 | 0.18 | -0.42 | -0.32 | -0.88 | -0.51 | -1.87 | -1.11 | -1.86 |

**Table S7.** Parameters of the multilinear regression $E_f(TM@TMC) = k + c_1E_f(TMC) + c_2E_f(TM)$. MAE and MSE stand for the mean absolute error and mean squared error, respectively. The multilinear regression has been performed with Scikit-learn.[38]

| | Parameter/Metric | Value | Standard error |
|---|---|---|---|
| Cubic TMCs | $k$ | -0.2461 | 0.021 |
| | $c_1$ | 0.3592 | 0.029 |
| | $c_2$ | 0.6010 | 0.030 |
| | R-squared | 0.877 | |
| | MAE | 0.336 | |
| | MSR | 0.199 | |
| Hexagonal TMCs | $k$ | 0.1147 | 0.088 |
| | $c_1$ | 0.2532 | 0.071 |
| | $c_2$ | 0.9540 | 0.069 |
| | R-squared | 0.732 | |
| | MAE | 0.550 | |
| | MSR | 0.639 | |

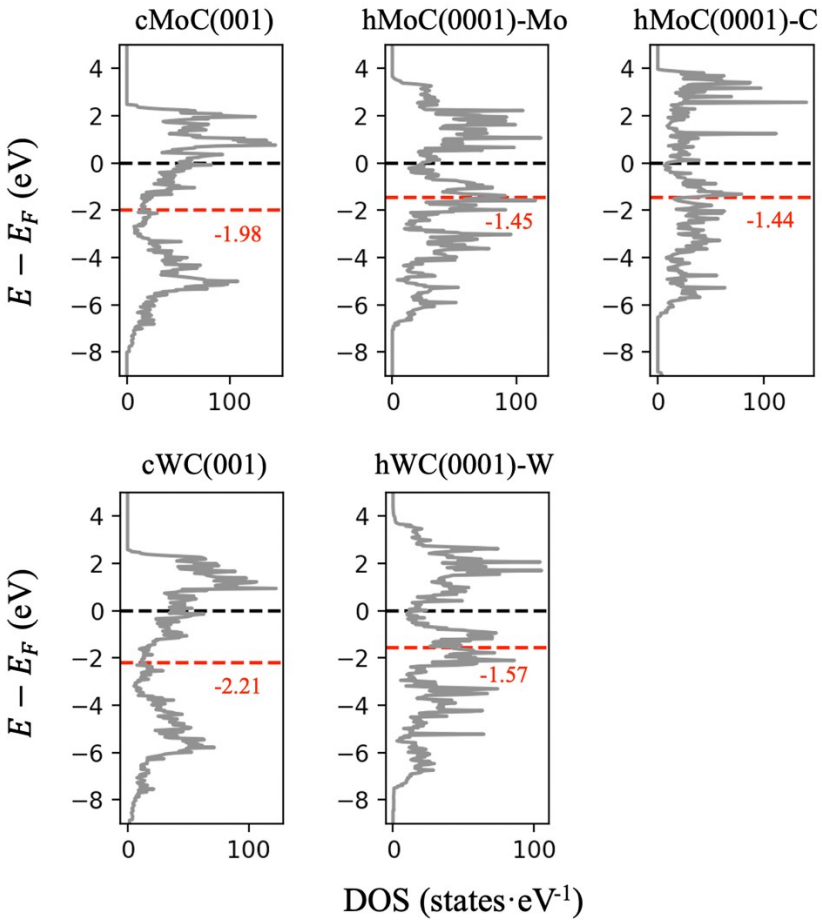


**Figure S2.** Partial density of states (DOS) plots for *d* electrons of selected systems. The red and black dashed lines represent the *d*-band centre and the Fermi level, respectively. We used the VASPKIT code[39] for post-processing of the VASP-calculated data.

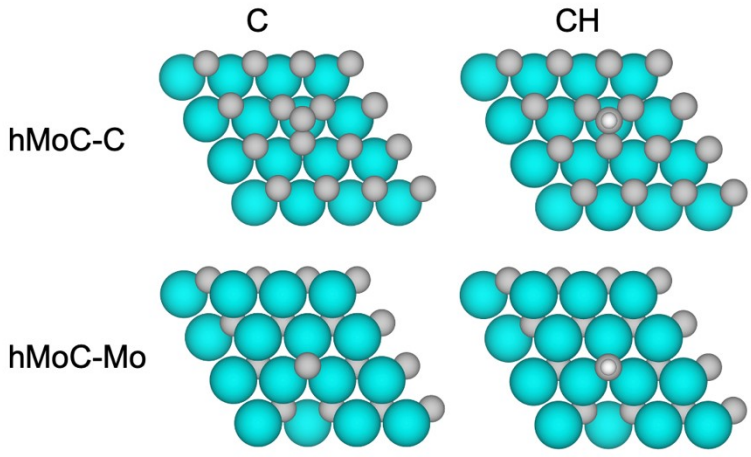


**Figure S3.** Top views of C (left) and CH (right) species adsorbed on the C-terminated (top) and Mo-terminated (bottom) hMoC(0001) slabs. While C and CH species form 3 C-C bonds with surface C atoms on the C-termination, they do not form C-C bonds in the Mo-termination.

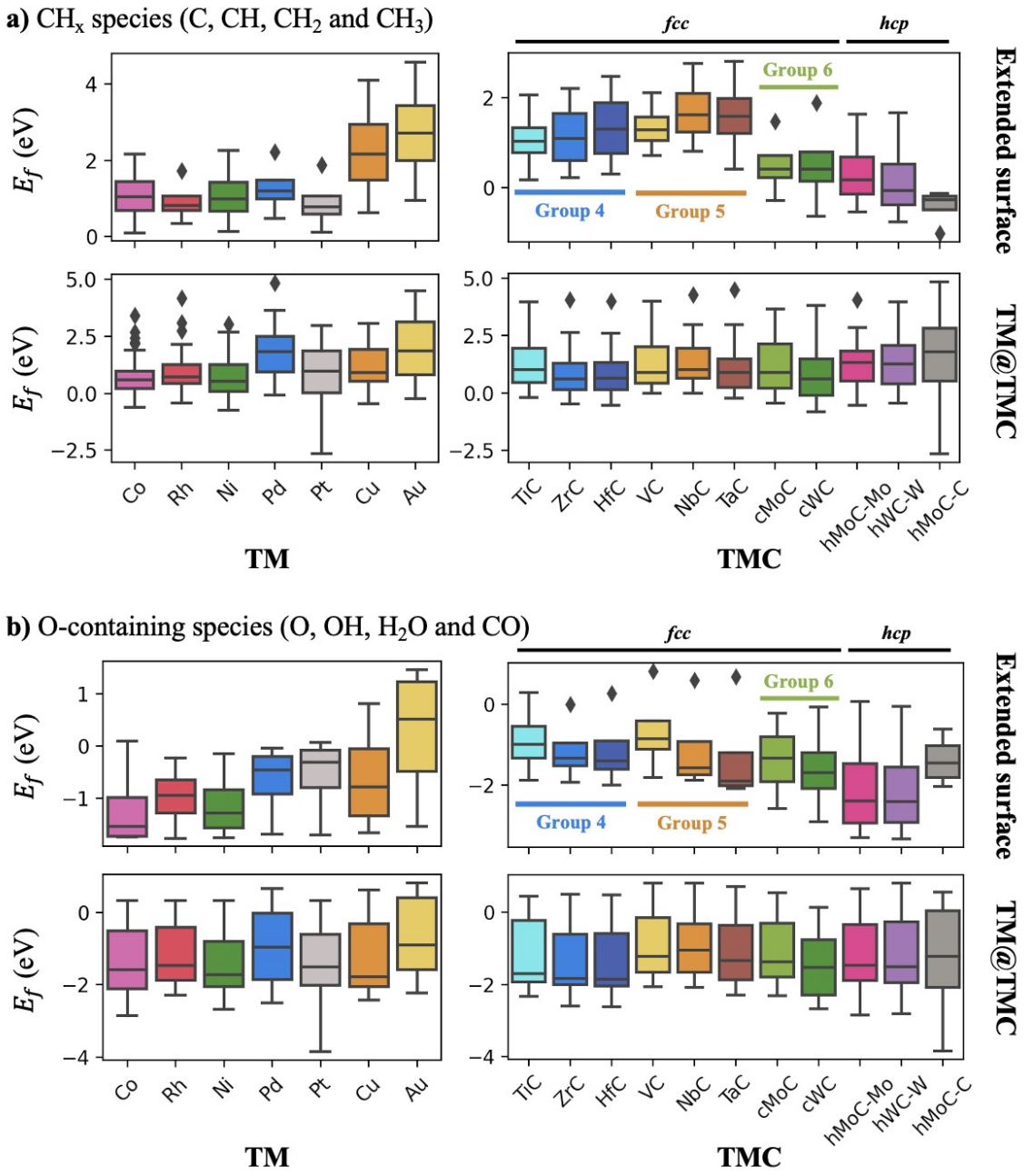


**Figure S4.** Box plots of the formation energies for $CH_x$ species (a) and O-containing species (b) on extended TM slabs (top left), extended TMC slabs (top right) and TM@TMC (bottom). The bottom plots show the distribution of formation energies on the supported clusters by cluster metal (left) and TMC support (right).

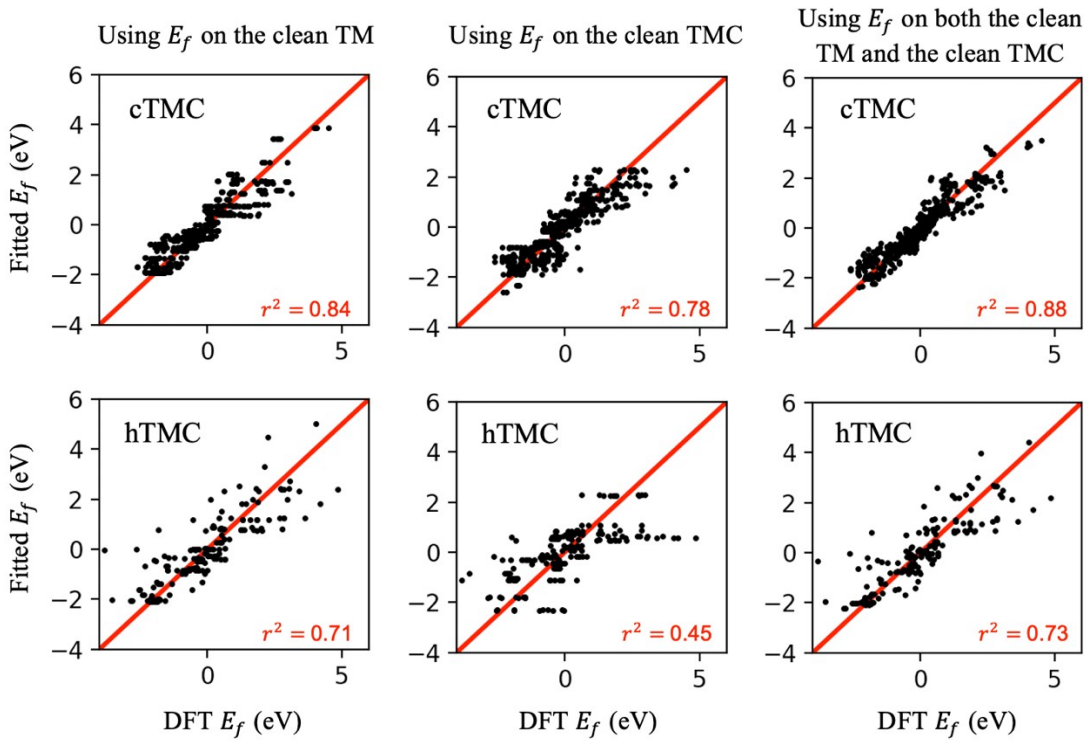


**Figure S5.** Parity plots of formation energies on TM@TMC (fitted versus computed by DFT) excluding those where the cluster displaces, deforms, or breaks.

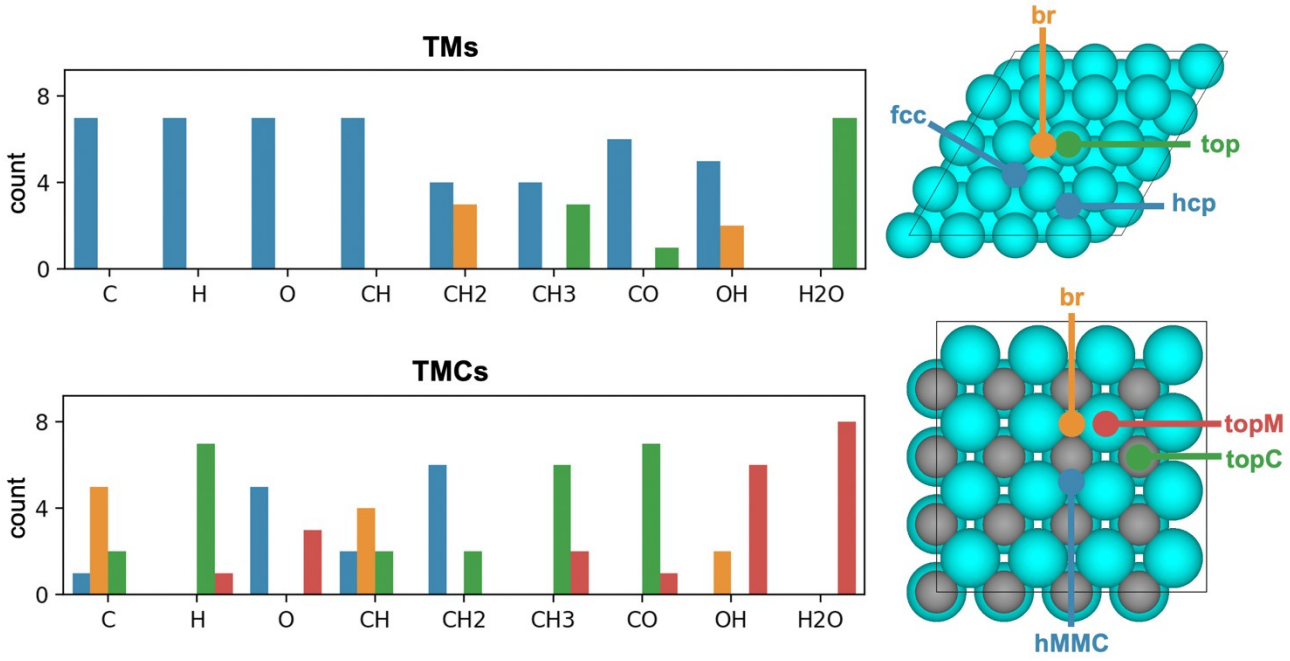


**Figure S6.** Distribution of preferred adsorption sites for adsorbed species on TM (top) and TMC (bottom) slabs. The right-side images show the location of the adsorption sites and the colours that correspond to each of them.

**Table S8.** Net Bader charges ($Q^{at}$) of surface C atoms for the cubic TMC(001) surfaces and the preferred adsorption sites for C, CH and $CH_2$ species.

| Facet | $Q^{at}$ C ($e$) | Preferred adsorption site | | |
|---|---|---|---|---|
| | | C | CH | $CH_2$ |
| cMoC(001) | -1.32 | br | br | hMMC |
| VC(001) | -1.39 | br | br | hMMC |
| cWC(001) | -1.43 | br | br | hMMC |
| TiC(001) | -1.58 | br | br | hMMC |
| NbC(001) | -1.60 | hMMC | br | hMMC |
| TaC(001) | -1.70 | hMMC | hMMC | hMMC |
| ZrC(001) | -1.78 | topC | topC | topC |
| HfC(001) | -1.82 | topC | topC | topC |

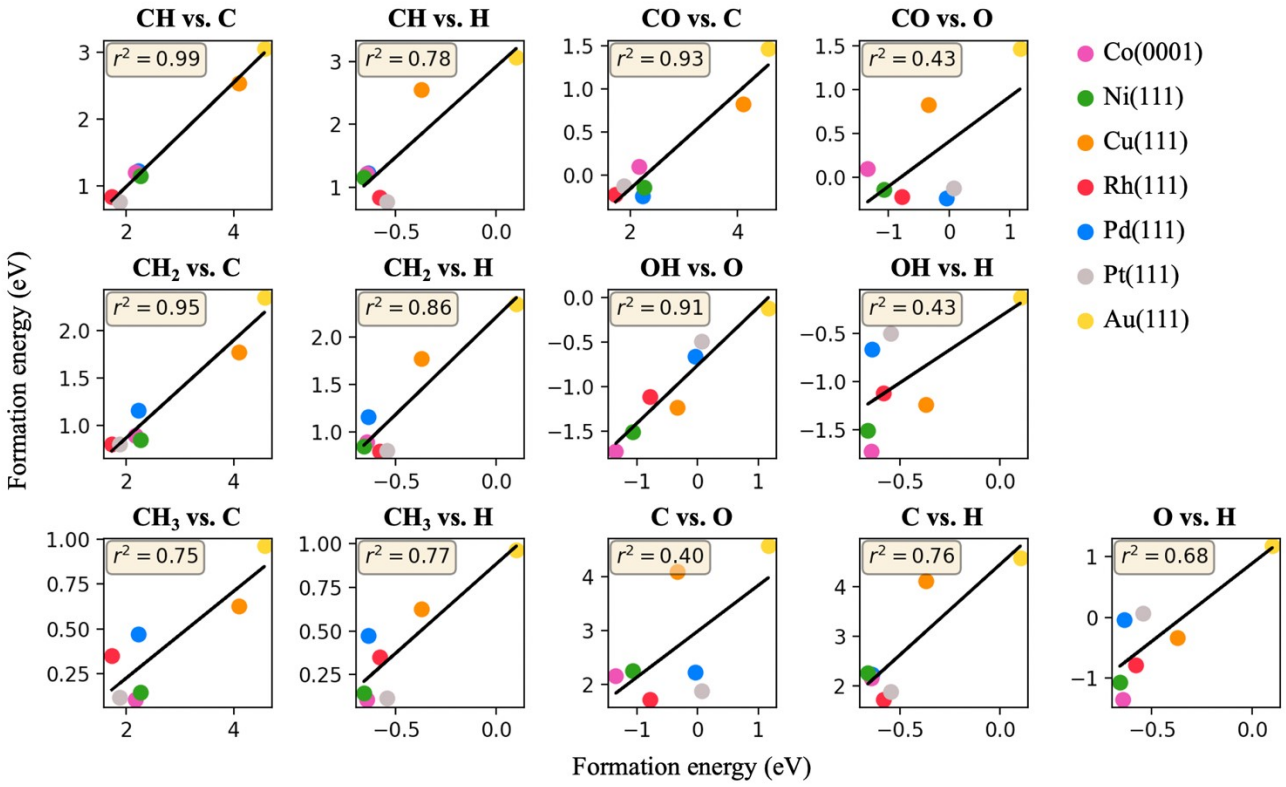


**Figure S7.** Linear scaling plots between the formation energies of different adsorbates on TM surfaces. Trend lines and R-squared coefficients are included.

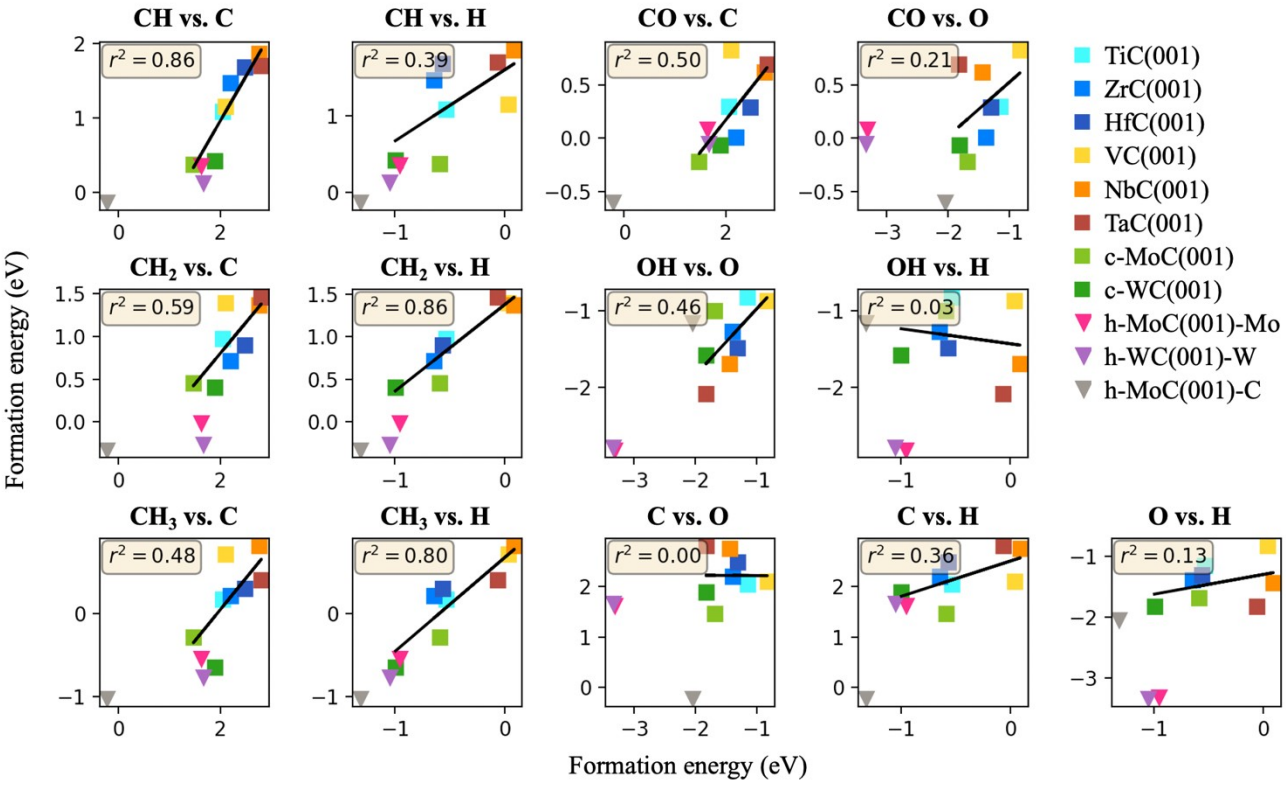


**Figure S8.** Linear scaling plots between the formation energies of different adsorbates on TMC surfaces. Trend lines and R-squared coefficients are included. Note that hexagonal TMCs (shown as triangles) have been excluded from the trend lines, as they exhibit different adsorption sites.

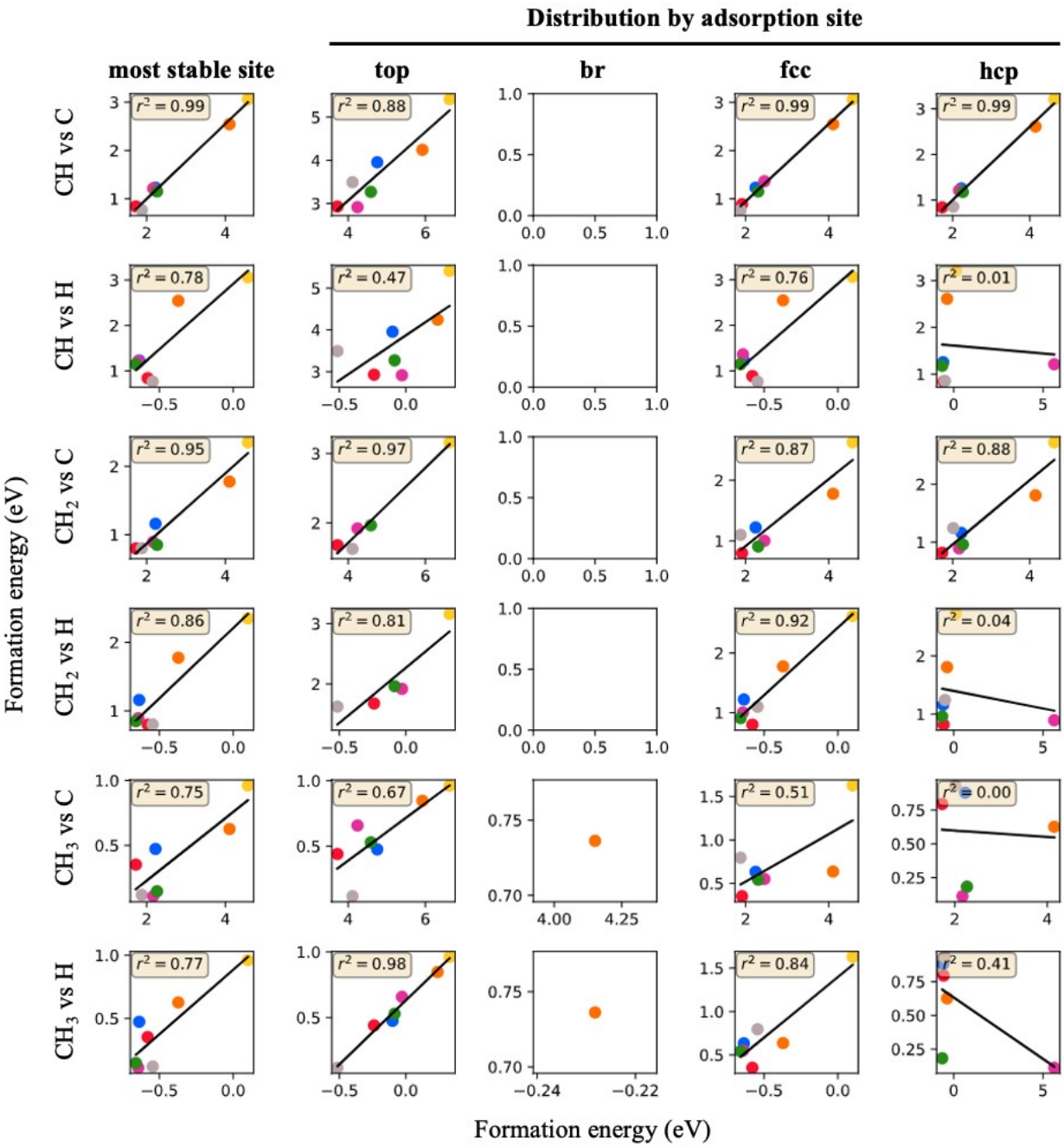


**Figure S9.** Linear scaling plots between the formation energies of different adsorbates on TM surfaces. Trend lines and R-squared coefficients are included. The plots on the first column correspond to the most stable adsorption site for each adsorbate, while the plots on the other columns correspond to a specific adsorption site (same for both adsorbates), which is indicated at the top.

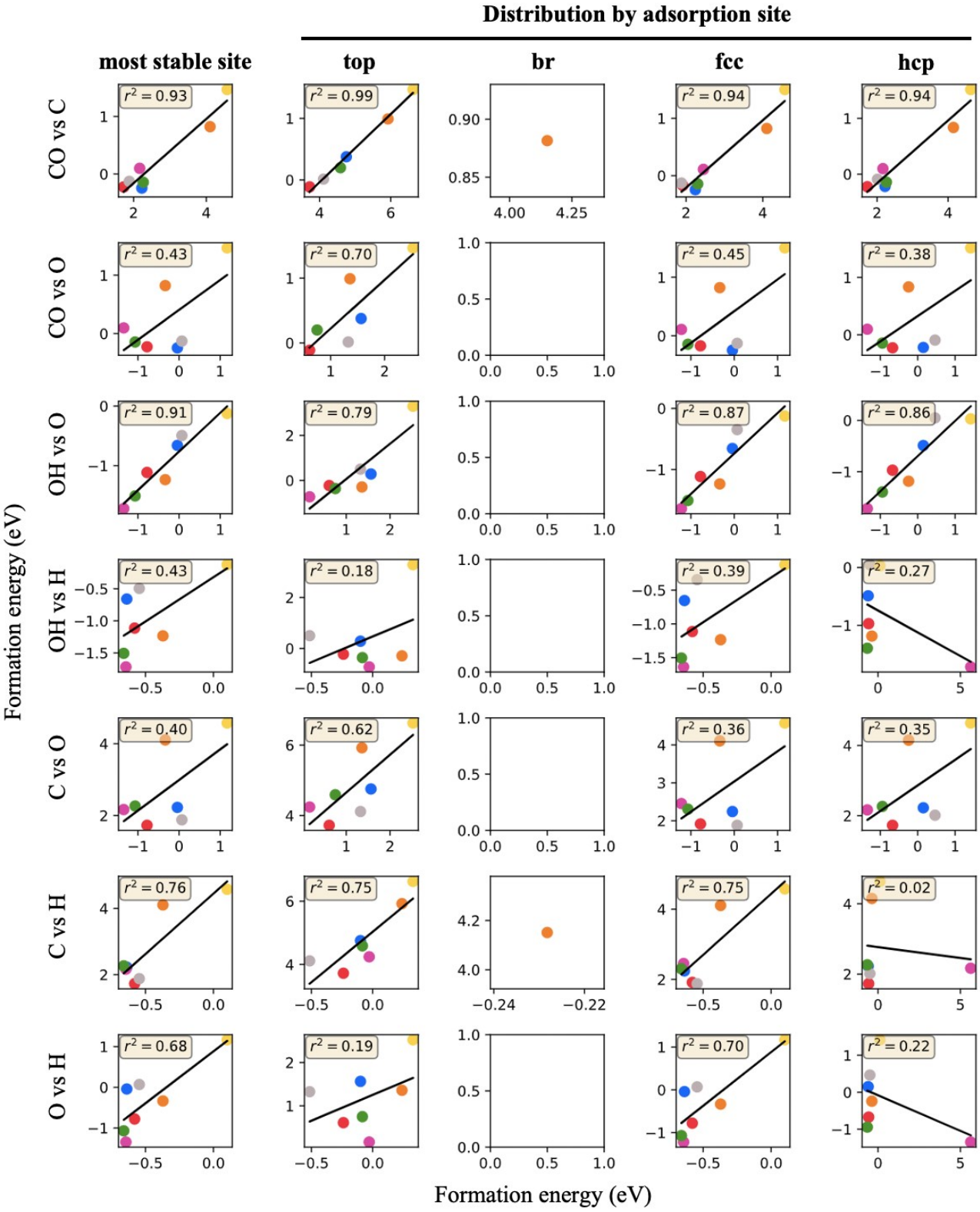


**Figure S9** (continued)

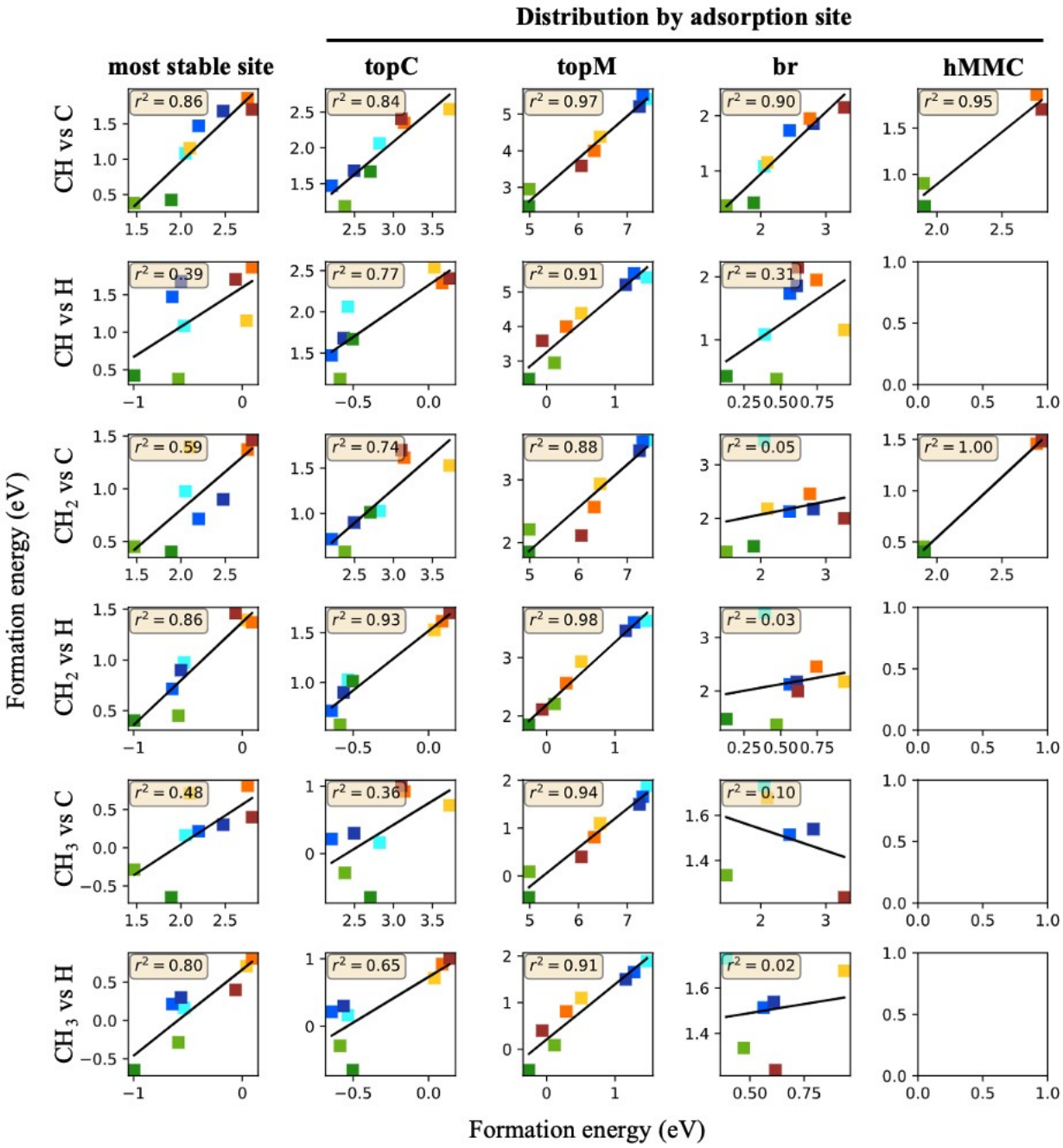


**Figure S10.** Linear scaling plots between the formation energies of different adsorbates on cubic TMC surfaces. Trend lines and R-squared coefficients are included. The plots on the first column correspond to the most stable adsorption site for each adsorbate, while the plots on the other columns correspond to a specific adsorption site (same for both adsorbates), which is indicated at the top.

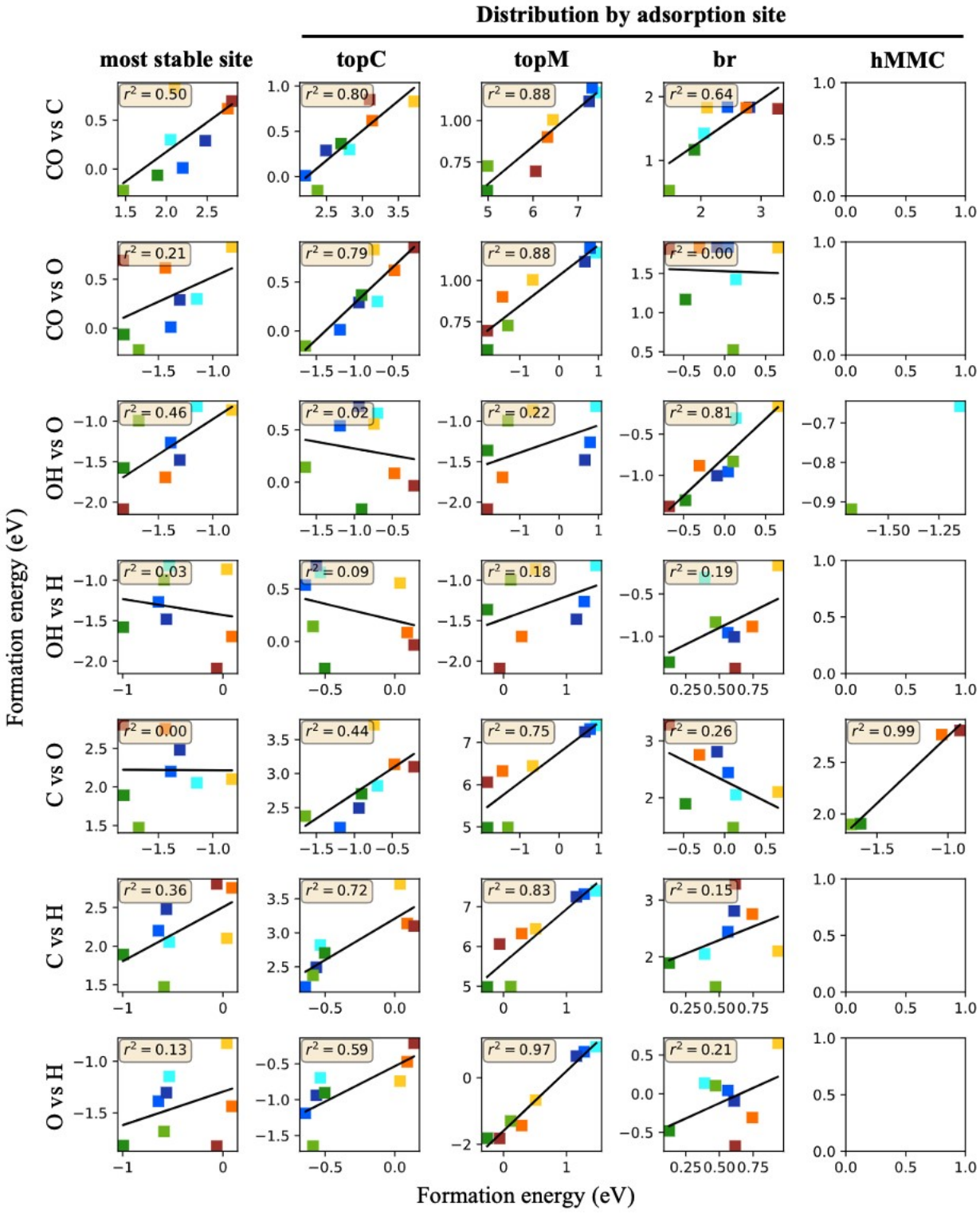


**Figure S10** (continued)

**References**


[1] G. Kresse and J. Furthmüller, *Phys. Rev. B* 1996, **54**, 11169–11186

[2] J. P. Perdew, K. Burke, M. Ernzerhof, *Phys. Rev. Lett*. 1996, **77**, 3865–3868

[3] P. Janthon, S. M. Kozlov, F. Viñes, J. Limtrakul and F. Illas, *J. Chem. Theory Comput.* 2013, **9**, 1631-1640

[4] S. Grimme, J. Antony and H. Krieg, *J. Chem. Phys.* 2010, **132**, 154104

[5] P. E. Blöchl, *Phys. Rev. B* 1994, **50**, 17953–17979

[6] G. Kresse and D. Joubert, *Phys. Rev. B* 1999, **59**, 1758–1775

[7] A. Jain, S. P. Ong, G. Hautier, W. Chen, W. D. Richards, S. Dacek, S. Cholia, D. Gunter, D. Skinner, G. Ceder and K. A. Persson, *APL Mater*. 2013, **1**, 011002

[8] S. P. Ong, W. D. Richards, A. Jain, G. Hautier, M. Kocher, S. Cholia, D. Gunter, V. Chevrier, K. A. Persson and G. Ceder, *Comp. Mater. Sci*. 2013, **68**, 314-319

[9] A. Hjorth Larsen, J. Jørgen Mortensen, J. Blomqvist, I. E. Castelli, R. Christensen, M. Dułak, J. Friis, M. N. Groves, B. Hammer, C. Hargus, E. D. Hermes, P. C. Jennings, P. B. Jensen, J. Kermode, J. R. Kitchin, E. L. Kolsbjerg, J. Kubal, K. Kaasbjerg, S. Lysgaard, J. B. Maronsson, T. Maxson, T. Olsen, L. Pastewka, A. Peterson, C. Rostgaard, J. Schiøtz, O. Schütt, M. Strange, K. S. Thygesen, Vegge, L. Vilhelmsen, M. Walter, Z. Zeng and K. W. Jacobsenet, *J. Phys. Condens. Matter.* 2017, **29**, 273002

[10] I. M. Billas, A. Châtelain and W. A. de Heer, *Science* 1994, **265**, 1682-4

[11] K. Nakamura and M. Yashima, *Mater. Sci. Eng., B* 2008, **148**, 69-72

[12] A. N. Christensen, *Acta Chem. Scand.* 1990, **44**, 851-852

[13] G. Will and R. Platzbecker, *Zeitschrift für Anorg. un Allg. Chemie.* 2001, **627**, 2207

[14] A. Chrysanthou and P. Greivson, *J. Mater. Sci. Lett.* 1991, **10**, 145-146

[15] A. Fernández-Guillermet, J. Häglund and G. Grimvall, *Phys. Rev. B: Condens. Matter Mater. Phys.* 1992, **45**, 11557-11567

[16] L. E. Toth, Transition Metal Carbides and Nitrides, Academic Press, New York, 1971

[17] J. Yang and F. Gao, *Phys. B* 2012, **407**, 3527-3534

[18] J. W. Arblaster, *Platinum Metals Rev.* 1997, **41**, 184

[19] J. W. Arblaster, *Platinum Metals Rev.* 2012, **56**, 181

[20] J. W. Arblaster, *Platinum Metals Rev.* 1997, **41**, 12

[21] V. K. Patel, Lattice constants, thermal expansion coefficients, densities, and imperfections in gold and the alpha-phase of the gold-indium system. Master's Thesis, 1967

[22] F. Vincent, M. Figlarz and C. R. Hebd, *Seances Acad. Sci*., 1967, **264C**, 1270

[23] A. Taylor, *J. Inst. Metals* 1950, **77**, 585

[24] L. S. Yu, *Acta Crystallogr*. 1969, **25A**, 676

[25] M. G. Quesne, A. Roldan, N. H. de Leeuw and C. R. A. Catlow, *Phys. Chem. Chem. Phys*. 2018, **20**, 6905-6916

[26] T. Xiao, A. P. E. York, K. S. Coleman, J. B. Claridge, J. Sloan, J. Charnock and M. L. H. Green, *J. Mater.*

*Chem*. 2001, **11**, 3094-3098

[27] D. J. Siegel, L. G. M. Hector Jr. and J. B. Adams, *Surf. Sci*. 2002, **498**, 321-336

[28] A. M. Nartowski, I. P. Parkin, M. MacKenzie, A. J. Craven and I. MacLeod, *J. Mater. Chem*. 1999, **9**, 1275-1281

[29] J. R. dos S. Politi, F. Viñes, J. A. Rodriguez and F. Illas, *Phys. Chem. Chem. Phys*. 2013, **15**, 12617-12625

[30] J. A. Rodriguez, J. Evans, L. Feria, A. B. Vidal, P. Liu, K. Nakamura and F. Illas, *J. Catal*. 2013, **307**, 162-169

[31] J. A. Rodriguez, L. Feria, T. Jirsak, Y. Takahashi, K. Nakamura and F. Illas, *J. Am. Chem. Soc.* 2010, **132**, 3177-3186

[32] J. A. Rodriguez, P. Liu, F. Viñes, F. Illas, Y. Takahashi and K. Nakamura, *Angew. Chem., Int. Ed.* 2008, **120**, 6787-6791

[33] J. A. Rodriguez, F. Viñes, F. Illas, P. Liu, Y. Takahashi and K. Nakamura, *J. Chem. Phys*. 2007, **127**, 211102

[34] H. Prats, R. A. Gutiérrez, J. J. Piñero, F. Viñes, S. T. Bromley, P. J. Ramírez, J. A. Rodriguez and F. Illas, *J. Am. Chem. Soc*. 2019, **141**, 5303-5313

[35] P. Lozano-Reis, H. Prats, R. Sayós, J. A. Rodriguez and F. Illas, *J. Phys. Chem. C* 2021, **125**, 12019-12027

[36] H. Prats and M. Stamatakis, *J. Mater. Chem. A.* 2022, **10**, 1522-1534

[37] F. Silveri, M. G. Quesne, F. Viñes, F. Illas, C. R. A. Catlow and N. H. de Leeuw, *J. Phys. Chem. C* 2022, **126**, 5138-5150

[38] F. Pedregosa, G. Varoquaux, A. Gramfort, V. Michel, B. Thirion, O. Grisel, M. Blondel, P. Prettenhofer, R. Weiss, V. Dubourg, J. Vanderplas, A. Passos, D. Cournapeau, M. Brucher, M. Perrot and E. Duchesnay, *J. Mach. Learn Res.* 2011, **12**, 2825-2830

[39] V. Wang, N. Xu, J.C. Liu, G. Tang and W.T. Geng, *Comp. Phys. Comm*, 2021, **267**, 108033